Supporting Information

Kim et al. 10.1073/pnas.1102650108

SI Text

Stack Design of InGaN/GaN Multiple Quantum Well (MQW) LED on Si(111) Substrate. Fig. S1 shows a schematic illustration of the epitaxial semiconductor multilayer stack of InGaN MQW LED on a Si(111) wafer. Active layers consist of a Si-doped n-GaN layer with a thickness of 1,700 nm, 5 layers of multiquantum well (MQW) of 3 nm InGaN and 10 nm of Si-doped GaN capped with Mg-doped p-GaN layer with a thickness of 110 nm. This wafer was purchased from Azzurro Semiconductor in Germany.

Fabrication Process of InGaN/GaN MQW μ-ILEDs on Flexible Substrates. Fig. S2 shows a schematic overview of the fabrication process. The process starts with InGaN epitaxial layers grown on Si (111) wafer, as illustrated in Fig. S1. For photolithography, photo-resist AZ5214-E was used as both a positive tone and negative tone resist. The steps for photolithography with this material appear below.

Photolithography using AZ5214-E as a positive-tone resist.

Spin-coat at 4,000 rpm for 30 s.
Prebake at 110 °C for 60 s.
Exposure dose of 78.5 mJ/cm^2 at 365 nm.
Develop in metal ion free (MIF) 327 for 35 s.
Hard bake at 130 °C for 180 s.
O_2 descuum for 45 s in 250 mTorr, 20 sccm of O_2 under 50 W.

Photolithography using AZ5214-E as a negative tone resist (image reversal).

Spin-coat at 5,000 rpm for 30 s.
Prebake at 110 °C for 60 s.
Exposure dose of 110 mJ/cm^2 at 320 nm
Postexposure bake (PEB) at 110 °C for 65 s.
Flood UV exposure of 400 mJ/cm^2.
Develop in MIF 327 for 35 s. More negatively sloped sidewalls can be achieved for easy lift-off if developed in MIF 327 for longer time (i.e., additional $10 \sim 15$ s).
O_2 descuum for 45 s in 250 mTorr, 20 sccm of O_2 under 50 W.

N-ohmic contact recession. P-GaN and MQW layers must be etched in the region where n-ohmic contacts are to be formed. First, n-ohmic contact regions are photo-lithographically defined using AZ positive-tone process (see *Photolithography using AZ5214-E as a positive tone resist*). Etching the GaN can be achieved using inductively coupled plasma reactive ion etching (ICP-RIE) with BCl_3 and Cl_2 gases, with pressures of 3 mTorr and temperatures of 25 °C. A two-step etching process was employed. The first step consisted of 15 sccm of BCl_3 with radio frequency (RF) power of 300 W and parallel plate DC voltage of 100 V for 90 s. The second step consisted of 15 sccm of Cl_2 gas with RF power of 300 W and parallel plate DC voltage of 100 V for an additional 120 s. An etch depth of 350 nm to 400 nm can be achieved with this recipe. After the ICP-RIE etching of GaN, the photo-resist (PR) was removed using acetone in an ultrasonic bath for about 120 s. The total etching depth was about 350 nm to 400 nm, as measured using profilometry.

N-ohmic contact deposition and annealing. Image Reversal of AZ5214-E [see *Photolithography using AZ5214-E as a negative tone resist (Image Reversal)*] and lift-off process were used to define n-ohmic contact metal. The native oxide on the surface n-GaN was removed using Buffered Oxide Etchant at a 10:1 mixing ratio for 120 s prior to metal deposition. (Ti:15 nm)/(Al:60 nm)/(Mo:20 nm)/(Au:100 nm) were evaporated at base pressures of 8×10^{-7} Torr as ohmic contacts to the n-GaN. An AG Associates Heatpulse 610 rapid thermal processor was used for rapid thermal annealing at 860 °C for 30 s under N_2 environment. Ohmic contact characteristics of Ti/Al/Mo/Au on n-GaN surface are described elsewhere (1).

P-ohmic contact deposition and annealing. Image reversal with AZ5214-E [see *Photolithography using AZ5214-E as a negative tone resist (Image Reversal)*] was used to define the p-ohmic contact regions. Immersion of p-GaN in HCl:DI = 3:1 for 5 min removed the native oxide. Ni (10 nm)/Au (10 nm) layers were deposited in an e-beam evaporator at a base pressure of $<5 \times 10^{-7}$ Torr at a relatively slow rate (approximately 0.5 A/s). After deposition, PR was removed using acetone in an ultrasonic bath for 120 s, and then Ni/Au layers were annealed in a furnace at 500 °C for 10 min in air (80% N_2 + 20% O_2) to improve the ohmic properties. Ohmic contact characteristics are depicted in Fig. S3.

Opaque contact pad. Image reversal with AZ5214-E [see *Photolithography using AZ5214-E as a negative tone resist (Image Reversal)*] was used to define the opaque contact pad regions on both p-ohmic contact region and n-ohmic contact region. Opaque contact pads served not only as contact electrodes, but also as mask patterns for the self-aligned passivation process, as illustrated in Fig. S5. As an opaque contact pad, Ti(10 nm)/Au(120 nm) was deposited using an e-beam evaporator. After deposition, PR was removed using acetone in an ultrasonic bath for 120 s.

SiN passivation layer deposition condition. SiN, which served as an etch barrier during the KOH undercut process, was deposited using an STS Multiplex plasma enhanced chemical vapor deposition (PECVD) system. Three hundred nm of SiN film was deposited at a pressure of 650 mTorr, temperature of 300 °C, and gas flow rates of 1,960 sccm (N_2) + 40 sccm (SiH_4) + 35 sccm (NH_3). Mixed frequency RF power of 20 W, with frequencies of 13.5 6 MHz for 6 s and 380 KHz for 2 s was used.

Ni etch mask deposition. On top of SiN film, AZ5214-E was used in an image reversal mode [see *Photolithography using AZ5214-E as a negative tone resist (Image Reversal)*] to define the lateral dimensions of the μ-ILEDs and the geometries of the anchors. Ti(50 nm)/Ni(450 nm) was deposited using an e-beam evaporator at relatively high deposition rate of approximately 6 A/s to minimize the thermal stress caused by the heating inside the chamber. After the deposition, PR was removed using acetone in an ultrasonic bath for 60 s.

SiN + GaN dry etching. SiN was dry-etched using a parallel plate RIE (Unaxis/Plasma Therm) with 40 sccm of SF_6, 35 mTorr pressure, and 100 W RF power, for an etch rate of SiN of ~100 nm/min. Upon the removal of SiN, GaN/InGaN/AlN/AlGaN epi-layers were all etched with a gas combination of $BCl_3/Cl_2/Ar$ in inductively coupled plasma reactive ion etching (ICP-RIE, Plasma Therm SLR770). Two etching steps were

incorporated in etching GaN/AlN based epitaxial layers, as in the following.

GaN etching step 1 in ICP-RIE.

Pressure: 5 mTorr.
Temperature: 25 °C.
Gas: 10 sccm of BCl_3 + 16 sccm of Cl_2 + 4 sccm of Ar.
ICP Coil power of 500 W and parallel plate voltage of 300 V.
Etching time: 1 min.

GaN etching step 2 in ICP-RIE.

Pressure: 5 mTorr.
Temperature of 25 °C.
Gas: 20 sccm of Cl_2 + 4 sccm of Ar.
ICP Coil RF power of 500 W and parallel plate voltage of 260 V.
Etching time: 8 additional min.

Anisotropic etching of silicon using KOH (Transene PSE-200).

Hot plate temperature: 100 °C.
Etching time: 45 min for a 100×100 μm^2 device.

Ti/Ni, SiN removal.

Ni etchant: (Transene TFB).
Etch rate: 3 nm/s at 25 °C.
SiN is dry etched using conditions described above.

Transfer-printing. Transfer-printing of μ-ILEDs was carried out onto either glass or PET substrates. Glass substrates were prepared by cleaving a slide into appropriate dimensions. PET substrates were prepared by spinning uncured poly(dimethylsiloxane) (PDMS) (10:1 mixture of base to curing agent) on a glass slide cleaved to appropriate dimensions at 2,000 rpm for 30 s. The PET film (Dura-Lar, Grafix) was laminated to the uncured PDMS and the entire substrate was cured at 70 °C for 3 h. A thin-film adhesive was spin-coated onto the secondary substrate after O_2 plasma at 3,000 rpm for 30 s and soft-baked at 110 °C for 10 min. Transfer-printing of μ-ILEDs was carried out in automated printer system using PDMS as a stamp. Step and repeat printing allowed formation of arrays with arbitrary configurations. The thin-film adhesive was cured under UV light for 10 min.

Self-aligned passivation by Back-side Exposure (BSE).

Adhesion promoter (AP3000) is spin-coated at 2,000 rpm for 30 s.
Soft-baking at 80 °C for 30 s.
BCB (Cyclotene 4024-40, Dow) is spin-coated at 2,000 rpm for 60 s.
Prebaking at 80 °C for 120 s.
Flood exposure dose from the back side of 123 mJ/cm^2 at 405 nm.
Postexposure baking (PEB) at 70 °C for 30 s.
Develop in DS2100 for 70 s.
Curing of BCB is carried out in oxygen-free environment at 210 °C for 60 min.
Descuum process using RIE at the pressure of 200 mTorr with 18 sccm of O_2 with 2 sccm of CF_4 with 150 W RF power for 30 s.

Metallization. Sputtered or e-beam evaporated Al was used for reflective interconnection. Aluminum was deposited and patterned photo-lithographically using AZ5214-E and an etch-back process (Type A, Transene). Fully interconnected arrays of μ-ILED resulted from this metallization process.

Ohmic Contact Characterization of Ni/Au Layers to p-GaN. Fig. S3 illustrates the ohmic contact characteristics of Ni(10 nm)/Au (10 nm) to p-GaN. Fig. S3*A* shows the current-voltage characteristics of Ni/Au contact to p-GaN with TLM pad spacings of 21 μm in three different annealing conditions (i.e., As deposited, 5 min annealing, 10 min annealing, and 15 min annealing). Fig. S3*B* shows a plot of total resistance at four different pad spacing ranging from 2.5 μm to 17 μm. The specific contact resistance could not be extracted due to the large sheet resistance associated with the highly resistive p-GaN. It is, however, qualitatively shown that 10 min annealing at 500 °C exhibits better ohmic characteristic than 15 min or 5 min annealing cases at the same temperature.

Versatility of Transfer-Printing Process. The versatility of the transfer-printing process is shown in Fig. S4 via corresponding SEM images of (*A*) after KOH undercut and (*B*) after transfer-printing. In Fig. S4*C*, μ-ILEDs are transfer-printed onto a glass substrate with varying pitches ranging from 25 μm to 500 μm.

Schematic for Passivation and Via Formation Using BSE Process. In Fig. S5*A*, a schematic illustration of an unusual passivation scheme using BSE process is shown. The self-aligned passivation starts with a transparent substrate such as a glass or a plastic. A transfer-printed μ-ILED exhibits transparency in wavelengths above its band-gap. First, a photosensitive polymer with a significant sensitivity (absorption) in the wavelength regime higher than the corresponding wavelength of the band-gap of GaN (~365 nm) is applied (e.g., by spin-coating) on the surface of printed μ-ILEDs. The polymer can effectively be crosslinked by the irradiation through the GaN and the substrate. The opaque contact pads serve as a masking layer. Corresponding SEM images of μ-ILEDs are shown in Fig. S5 *B* and *C* with 100× 100 μm^2 device and in Fig. S5*D* with 25×25 μm^2 device after the BSE process. Cross-sectional profiles of a passivated μ-ILED (acquired using profilometry) are shown in Fig. S5*E*. This process naturally generates vias with positive sidewall.

Uniformity in Electrical Properties of μ-ILED on Mechanical Deformation. Fig. S6 *A* and *B* show electrical properties (I–V characteristics and forward voltage at 10 mA of current) for representative μ-ILEDs printed on a PET substrate measured for varying bending radii and repetitive cycles. These I–V data demonstrate that the μ-ILEDs do not change in an appreciable way to bending radii down to ~5.9 mm and up to 1,000 bending cycles. For this specific substrate configuration, these results indicate robust operation of the devices to strains up to 0.18%.

Uniformity in Electrical Properties of μ-ILED in an Array. Current-voltage characteristics of 100 μ-ILEDs from an array, shown in Fig. S7*A*, exhibit excellent uniformity. For example, less than 100 mV difference in the forward voltage is shown at 3 mA current. An array consists of 100 μ-ILEDs in a hexagonal arrangement (e.g., equal spacing between all μ-ILEDs) are shown in Fig. S7*B*.

Integration YAG:Ce Phosphors with μ-ILED in an Array. Phosphors must be dispersed uniformly to generate uniform white light. Fig. S8*A* shows optical microscope images of relief features filled with a PDMS/phosphor slurry (left column) and filled with the phosphor powder only (right column). Compared to the "dry filling" method, the PDMS/phosphor slurry provides excellent dispersion and uniformity of phosphor in the PDMS matrix. Emission spectra of white μ-ILEDs are shown in Fig. S8*B* with phosphor layer thicknesses of 60 μm, 80 μm, and 105 μm.

Fabricating SU-8 mold for phosphor-island mold.

Spin-coat SU-8 5 on Si(100) wafer 1,800 rpm for 30 sec.

Bake at 95 °C for 5 min.
Flood exposure dose of 216 mJ/cm^2 at 365 nm.
Spin SU-8 50 and expose.

For 60 μm film: Spin 1,800 rpm for 30 sec, Exposure dose of 432 mJ/cm^2 at 365 nm.
For 80 μm film: 1,600 rpm for 30 sec, Exposure dose of 513 mJ/cm^2 at 365 nm.
For 105 μm film: 1,250 rpm for 30 sec, Exposure dose of 583 mJ/cm^2 at 365 nm.
Bake at 65 °C for 1 min then ramp to 95 °C, total bake time 11 min.
Develop in SU-8 Developer 12 min.
Bake 180 °C for 10 min.
UVO treatment for 2 min.
Treat with tridecafluoro-1,1,2,2-tetrahydrooctyl trichlorosilane for 2 h in air-tight container.

Creating white light, μ-ILED.

Cast 10 : 1 mixture (base to curing agent) of uncured PDMS over SU-8 master.
Cure at 70 °C for 3 h.
Create phosphor/PDMS slurry: Mix 37.35 wt% phosphor in 10 : 1 PDMS with glass stir rod.
Drip small amount of slurry on PDMS mold.
With PDMS-coated razor blade, squeegee slurry into relief features of PDMS mold.
Repeat in orthogonal direction.
Cure at 70 °C for 3 h.
Phosphor-island mold is manually aligned to the back side of a function μ-ILED array.

Analytical Model of Printed μ-ILED on a Glass Substrate. ***Basic equations.*** A half space with built-in disk heat source is used to model the present problem. The cylindrical coordinate system is set such that the origin is coincident with the center of the heat source. Schematic illustration of the device geometry and parameters used in the analytical model of heat flow is shown in Fig. S9. The steady-state axisymmetric heat conduction in cylindrical coordinates is

$$\frac{\partial^2 T}{\partial r^2}+\frac{1}{r}\frac{\partial T}{\partial r}+\frac{\partial^2 T}{\partial z^2}=0. \qquad \textbf{[S1]}$$

Setting $\theta = T - T_\infty$, where T_∞ is the remote temperature, the above equation is equivalent to

$$\frac{\partial^2 \theta}{\partial r^2}+\frac{1}{r}\frac{\partial \theta}{\partial r}+\frac{\partial^2 \theta}{\partial z^2}=0. \qquad \textbf{[S2]}$$

Boundary and continuity conditions are as follows:

1. $z = -H_g - H_L = h_1$ (Glass bottom surface):

$$\theta_g|_{z=h_1}=0. \qquad \textbf{[BC1]}$$

2. $z = 0$ (BCB-glass interface):
Downward heat flux

$$-k_b\frac{\partial \theta_b}{\partial z}\bigg|_{z=0}=G_1(r)=\begin{cases}-q_1, & 0\le r\le r_0\\ q_{0,\mathrm{int}}, & r>r_0\end{cases}. \qquad \textbf{[a]}$$

Upward heat flux

$$-k_g\frac{\partial \theta_g}{\partial z}\bigg|_{z=0}=G_2(r)=\begin{cases}q_2, & 0\le r\le r_0\\ q_{\mathrm{b,int}}, & r>r_0\end{cases}. \qquad \textbf{[b]}$$

Here the heat flux satisfy the following conditions

$$q_1\pi r_0^2+q_2\pi r_0^2=Q, \qquad \textbf{[c]}$$

$$\theta_g\Big|_{z=0}=\theta_b\Big|_{z=0}, \qquad \left[-k_b\frac{\partial \theta_b}{\partial z}\right]_{z=0,r\ge r_0}=\left[-k_g\frac{\partial \theta_g}{\partial z}\right]_{z=0,r\ge r_0}, \qquad \textbf{[BC2]}$$

where k_g and k_b are the thermal conductivities of glass and BCB, r_0 is the equivalent radius of LED and Q is the total heat generated in the LED.

3. $z = H_b = h_2$ (BCB-interconnect interface):

$$\theta_b\Big|_{z=h_2}=\theta_m\Big|_{z=h_2}, \qquad -k_b\frac{\partial \theta_b}{\partial z}\bigg|_{z=h_2}=-k_m\frac{\partial \theta_m}{\partial z}\bigg|_{z=h_2}, \qquad \textbf{[BC3]}$$

where k_m is the thermal conductivity of metal interconnect.

4. $z = H_b + H_m = h_3$ (Interconnect-air interface):

$$-k_m\frac{d\theta_m}{dz}\bigg|_{z=h_3}=h\theta_m|_{z=h_3}, \qquad \textbf{[BC4]}$$

where h is the coefficient of convection at the upper surface of a plate.

Solution. Eq **2** is solved via the Hankel transform, for which the following transform pair of the first kind is used,

$$\varphi(r,z)=\int_0^\infty \bar{\varphi}(\xi,z)J_0(\xi r)\xi d\xi$$
$$\bar{\varphi}(\xi,z)=\int_0^\infty \varphi(r,z)J_0(\xi r)r dr, \qquad \textbf{[S3a,b]}$$

where $\varphi(r,z)$ is the original function and $\bar{\varphi}(\xi,z)$ is the transform. The Hankel transform of **[2]** is

$$\frac{d^2\bar{\theta}}{dz^2}-\xi^2\bar{\theta}=0 \qquad \textbf{[S4]}$$

for which the solution is obtained as

$$\bar{\theta}=Ae^{-\xi z}+Be^{\xi z}, \qquad \textbf{[S5]}$$

and the heat flux is

$$-k\frac{\partial \bar{\theta}}{\partial z}=k\xi(Ae^{-\xi z}-Be^{\xi z}), \qquad \textbf{[S6]}$$

where A and B are two unknown functions to be determined according to boundary and continuity conditions. The temperature and heat flux are obtained as

$$\theta=\int_0^\infty (Ae^{-\xi z}+Be^{\xi z})J_0(\xi r)\xi d\xi \qquad \textbf{[S7]}$$

$$q_z=-k\frac{\partial \theta}{\partial z}=\int_0^\infty k\xi(Ae^{-\xi z}-Be^{\xi z})J_0(\xi r)\xi d\xi. \qquad \textbf{[S8]}$$

The boundary and continuity conditions can also be expressed in Hankel transform. Using **[5–8]**, the two unknowns A and B for each layer can be solved. For glass,

$$A_g=\frac{1}{\beta_1-\beta_2 e^{-2\xi h_1}}\frac{(\kappa+1)}{k_b\xi}\frac{Q}{\pi r_0}\frac{J_1(\xi r_0)}{\xi} \qquad B_g=-A_g e^{-2\xi h_1}. \qquad \textbf{[S9]}$$

For BCB,

$$A_b = \frac{1}{2}\left(1+\frac{k_g}{k_b}\right)A_g + \frac{1}{2}\left(1-\frac{k_g}{k_b}\right)B_g + \frac{1}{2k_b\xi}\frac{Q}{\pi r_0}\frac{J_1(\xi r_0)}{\xi}$$
$$B_b = \frac{1}{2}\left(1-\frac{k_g}{k_b}\right)A_g + \frac{1}{2}\left(1+\frac{k_g}{k_b}\right)B_g - \frac{1}{2k_b\xi}\frac{Q}{\pi r_0}\frac{J_1(\xi r_0)}{\xi}. \quad \textbf{[S10]}$$

For interconnect,

$$A_m = \frac{1}{2}\left[\left(1+\frac{k_b}{k_m}\right)A_b e^{-2\xi h_2} + \left(1-\frac{k_b}{k_m}\right)B_b\right]e^{2\xi h_2}$$
$$B_m = \frac{1}{2}\left[\left(1-\frac{k_b}{k_m}\right)A_b e^{-2\xi h_2} + \left(1+\frac{k_b}{k_m}\right)B_b\right], \quad \textbf{[S11]}$$

where

$$\beta_1 = \left(1-\frac{k_g}{k_b}\right) - \left(1+\frac{k_g}{k_b}\right)\kappa,$$
$$\beta_2 = \left(1+\frac{k_g}{k_b}\right) - \left(1-\frac{k_g}{k_b}\right)\kappa$$
$$\kappa = \frac{\left(1-\frac{k_b}{k_m}\right)e^{-2\xi h_3} - \frac{k_m\xi-h}{k_m\xi+h}e^{-2\xi h_3}\left(1+\frac{k_b}{k_m}\right)}{\frac{k_m\xi-h}{k_m\xi+h}e^{-2\xi h_3}\left(1-\frac{k_b}{k_m}\right)e^{2\xi h_3} - \left(1+\frac{k_b}{k_m}\right)}. \quad \textbf{[S12]}$$

The temperature in each layer can be obtained by Eq. **S7**. For example, the temperature in interconnect is given by

$$T_m(r,z) = T_\infty + \int_0^\infty (A_m e^{-\xi z} + B_m e^{\xi z}) J_0(\xi r)\xi d\xi. \quad \textbf{[S13]}$$

The interconnect surface temperature is then obtained by setting $z = h_3$. The LED temperature can be approximately by its average value over the entire active region as

$$T_{LED} = T_\infty + \frac{2}{r_0}\int_0^\infty (1-e^{-2\xi h_1})A_g J_1(\xi r_0)d\xi. \quad \textbf{[S14]}$$

The thermal conductivity of Al decreases as the film thickness decreases (2–5) as shown in Fig. S10*A*, which is extracted from several references. For our model, the thermal conductivity of Al is used as a fitting parameter, but with constraints to approximate the literature values. In the case of 300 nm and 1,000 nm Al interconnects, the thermal conductivities of 70 W/m/k and 160 W/m/k, respectively, are used in the model. These values were compared with reported values from the literatures to make sure they are within the reasonable range as depicted in Fig. S10*A*.

Finite Element Model to Determine the Temperature Distribution. A three-dimensional finite element model is established to study the temperature distribution in the LED system and validate the analytical model. Eight-node, hexahedral brick elements in the finite element software ABAQUS are used to discretize the geometry. A volume heat source is applied on the LED. The thermal convection boundary is applied at the air-interconnect interface and a constant temperature is applied at the bottom of the glass substrate. For LED arrays, a $\frac{1}{4}$ unit cell is used to take advantage of symmetry and periodic boundaries are applied. The finite element simulations agree well with analytical modeling as shown in Fig. S10*D*.

Experimental Setup for Measuring the LED Temperature. The printed μ-ILED is placed on a heated chuck with a base temperature of 50 °C, and pixel-by-pixel calibration is performed to yield a reference irradiance image of an unpowered sample in order to account for the emissivity differences on the sample surface. In some cases, however, when the material has emissivity <0.1, such as Al, temperature measurement could be inaccurate due to very low thermal emission (6). A surface ink or polymer that emits as a blackbody can be placed on top of the sample and to eliminate variation in emissivity (7). We did not use this procedure because of the destructive nature of this material to electrical device. As a result, we extracted quantitative values for the temperature only at the open areas between Al interconnects.

1. Kumar V, Zhou L, Selfanathan D, Adesida I (2002) Thermally stable low-resistance Ti/Al/Mo/Au multilayer ohmic contacts on n-GaN. *J Appl Phys* 92:1712–1714.
2. Bourgoin JP, Allogho GG, Hache A (2010) Thermal conduction in thin films measured by optical surface thermal lensing. *J Appl Phys* 108:073520.
3. Schmidt AJ, Cheaito R, Chiesa M (2010) Characterization of thin metal films via frequency-domain thermoreflectance. *J Appl Phys* 107:024908.
4. Spina LL, et al. (2006) MEMS test structure for measuring thermal conductivity of thin films. *Proc IEEE International Conference on Microelectronic Test Structures* Austin, TX, 137–142.
5. Stojanovic N, et al. (2007) Thin-film thermal conductivity measurement using microelectrothermal test structures and finite-element-model-based data analysis. *J Microelectromech S* 16:1269–1275.
6. Webb PW (1991) Thermal imaging of electronic devices with low surface emissivity. *Proc Inst Electr Eng* 138:390–400.
7. Sarua A, et al. (2006) Combined infrared and raman temperature measurements on device structures. *CS Mantech Conf* Vancouver, British Columbia, Canada, 179–182.

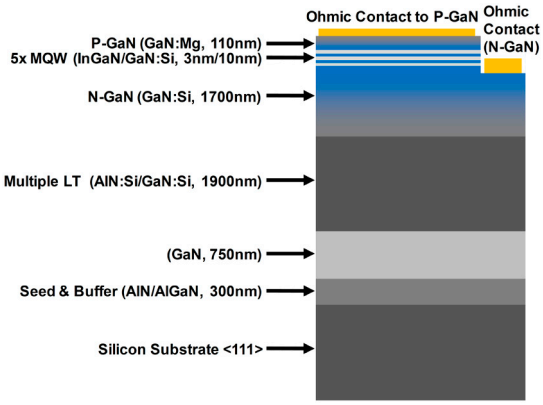

Fig. S1. Schematic illustration of epitaxial stack of InGaN MQW LED on Si (111) wafer.

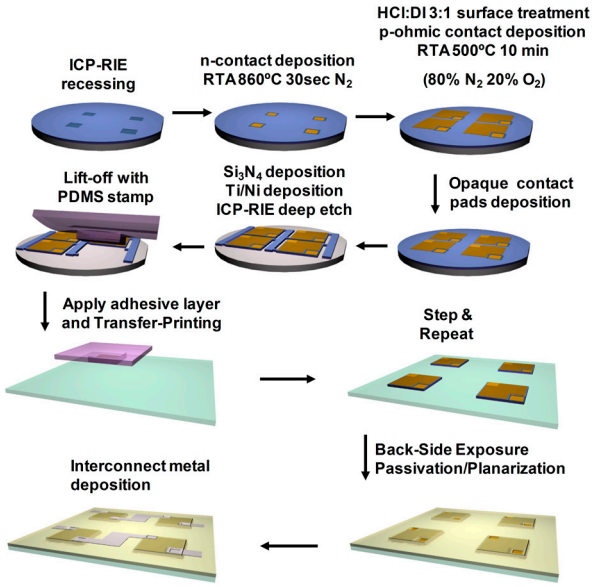

Fig. S2. Schematic overview of the fabrication process.

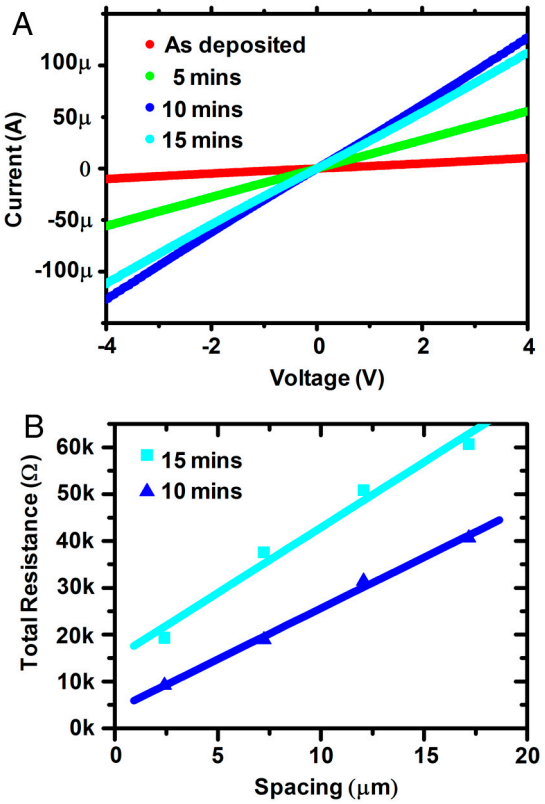

Fig. S3. Ohmic contact characteristics of Ni(10 nm)/Au(10 nm) to p-GaN. (*A*) Current-voltage characteristics of Ni/Au contact to p-GaN with TLM pad spacing of 21 μm in three different annealing conditions (i.e., As deposited, 5 min, 10 min, and 15 min annealing). (*B*) Plot of total resistance at four different pad spacing of 2.5 μm, 7.25 μm, 12 μm, and 17 μm.

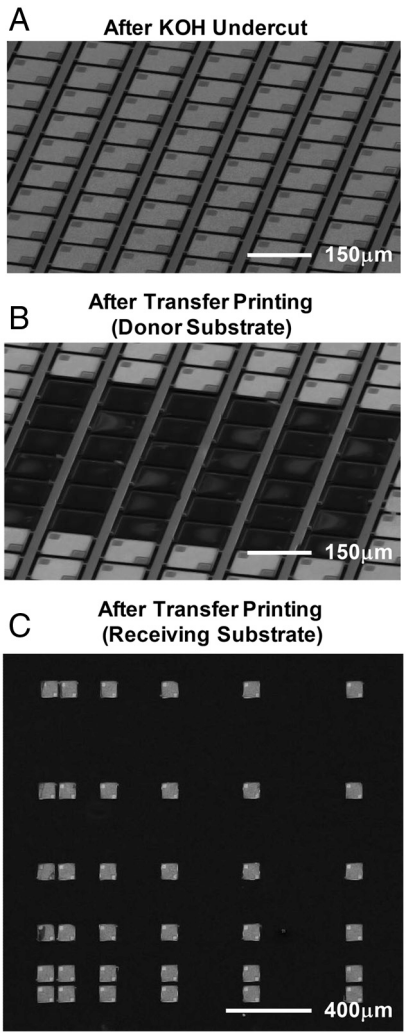

Fig. S4. SEM images of μ-ILEDs on (*A*) donor substrate after KOH undercut process, (*B*) donor substrate after transfer-printing process, and (*C*) receiving substrate (i.e., glass) after the transfer-printing process. μ-ILEDs are transfer-printed onto a glass substrate with varying pitches ranging from 25 μm to 500 μm.

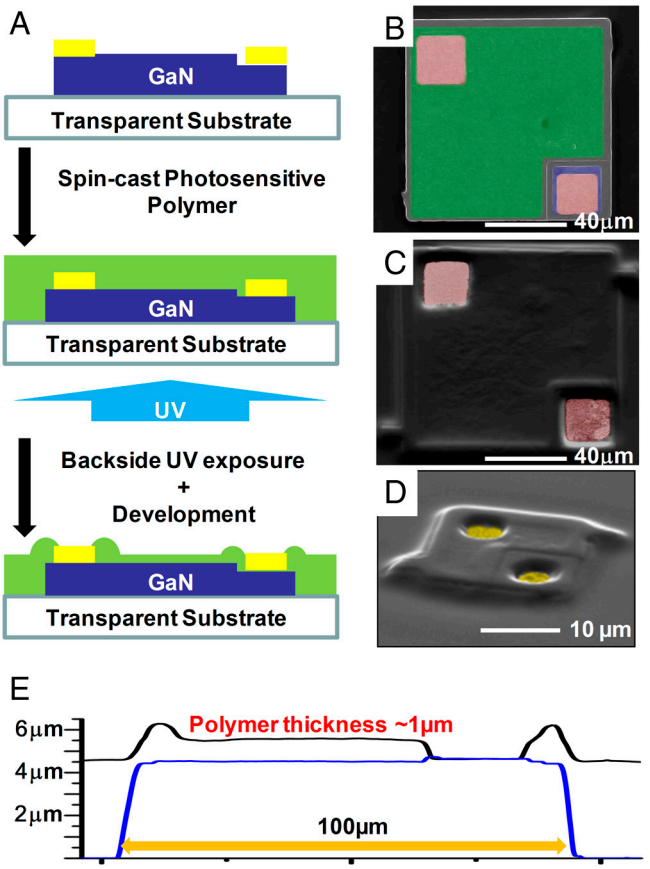

Fig. S5. (*A*) Schematic illustration of BSE process for self-aligned passivation and via formation. SEM image of a 100×100 μm^2 printed μ-ILED (*B*) before, and (*C*) after BSE process. (*D*) SEM image of 25×25 μm^2 μ-ILED after BSE process (colorized for easy of viewing). (*E*) Cross-sectional profile of μ-ILEDs after BSE process.

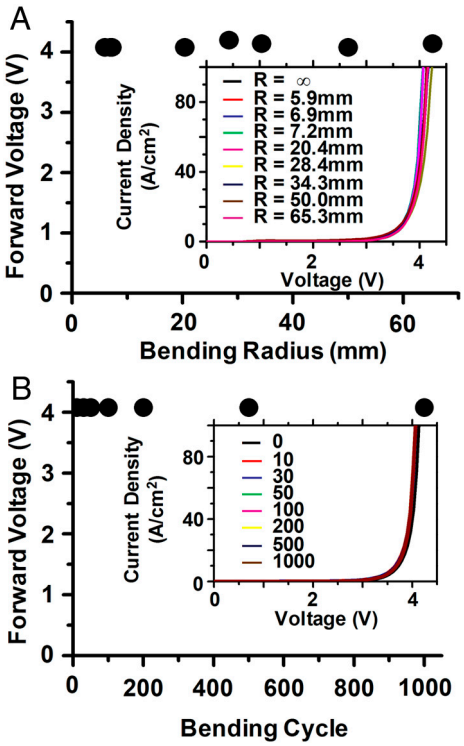

Fig. S6. (*A*) Forward voltage at 10 mA of current and corresponding current-voltage characteristics (inset) for representative μ-ILEDs printed on a PET substrate measured for varying bending radii. (*B*) Forward voltage at 10 mA of current and corresponding current-voltage characteristics (inset) for representative μ-ILEDs printed on a PET substrate measured for repetitive cycles.

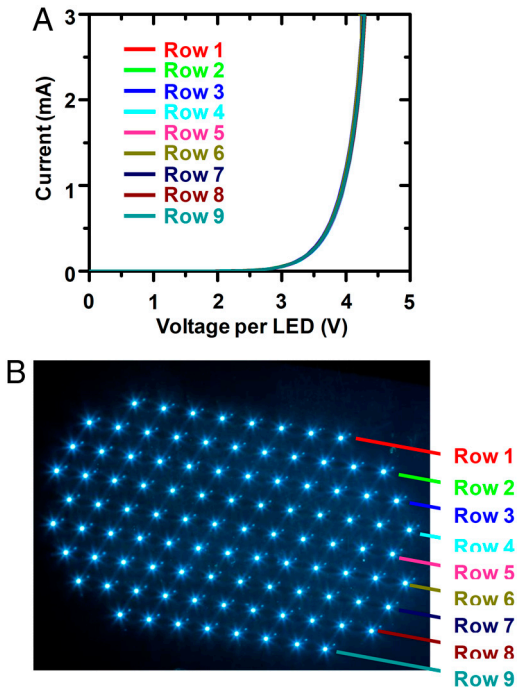

Fig. S7. (*A*) Current-voltage (I-V) characteristics of 100 μ-ILEDs from an array. (*B*) Optical image of an array consists of 100 μ-ILEDs.

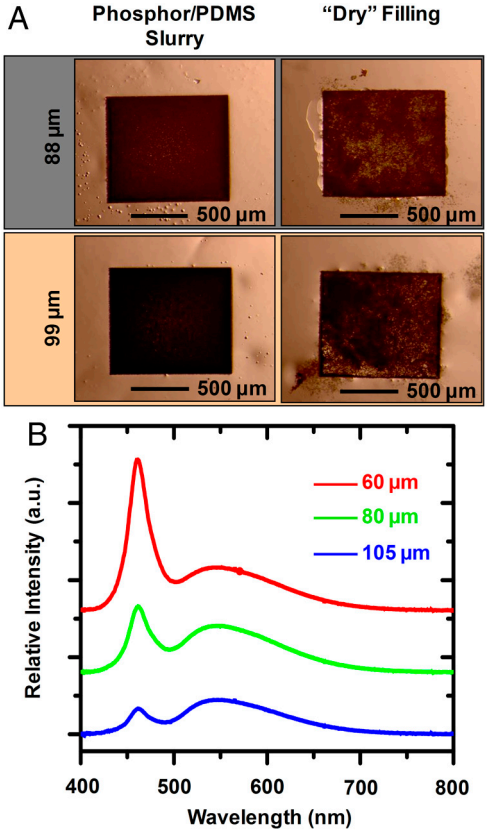

Fig. S8. (*A*) Optical microscopy images of relief features filled with a PDMS/phosphor slurry (left column) and filled with the phosphor powder only (right column). (*B*) Emission spectra of white μ-ILEDs with phosphor layer thickness of 60 μm, 80 μm, and 105 μm.

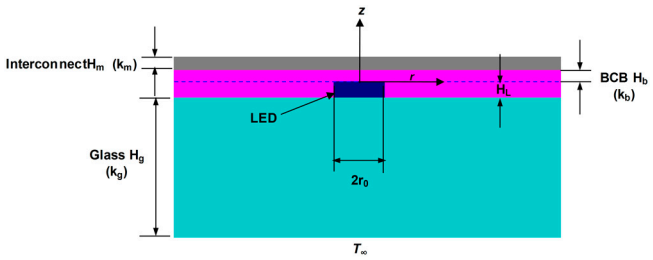

Fig. S9. Schematic illustration of the device geometry and parameters used in the analytical model of heat flow.

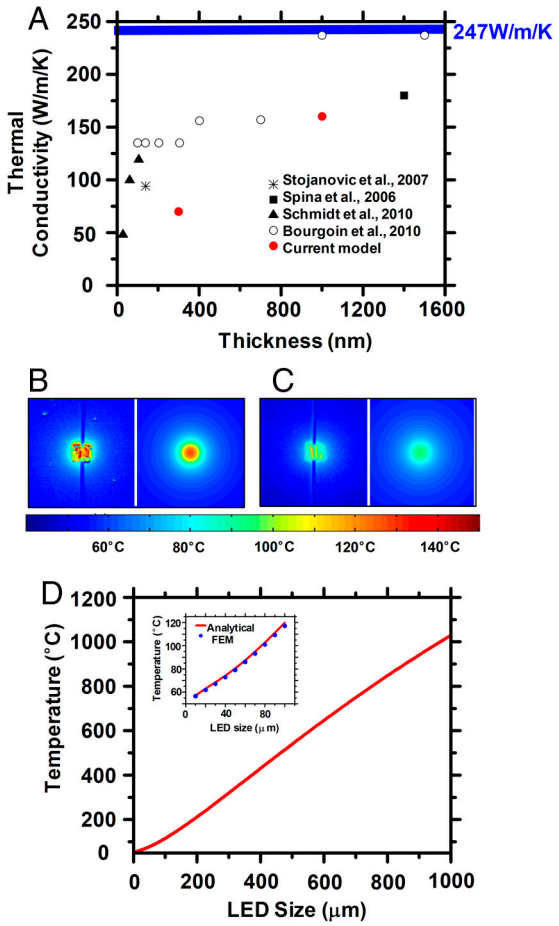

Fig. S10. (*A*) Reported thermal conductivities of a thin-film Al from several references. (*B–C*) Temperature distributions for isolated InGaN μ-ILEDs with Al interconnects [300 nm and 1,000 nm thick for (*B*) and (*C*), respectively] at input powers of (*B*) 25.2 mW and (*C*) 27.6 mW captured using a QFI Infra-Scope Micro-Thermal Imager (left) and calculated by analytical models (right). (*D*) A plot from analytical results on the surface temperature as function of LED size up to 1×1 mm^2. Inset provides comparison between analytical solution and FEM simulations on the surface temperature as function of LED size ranging from 10×10 μm^2 up to 100×100 μm^2.